

Formation of Stable Radicals by Mechanochemistry and Their Application for Magic Angle Spinning Dynamic Nuclear Polarization Solid-State NMR Spectroscopy

Scott L. Carnahan,* Kipper Riemersma, Ihor Z. Hlova, Oleksandr Dolotko, Steven J. Kmiec, Sujeewa N. S. Lamahewage, Steve W. Martin, James F. Wishart, Thierry Dubroca, Viktor P. Balema, and Aaron J. Rossini*



Cite This: *J. Phys. Chem. A* 2024, 128, 3635–3645



Read Online

ACCESS |



Metrics & More

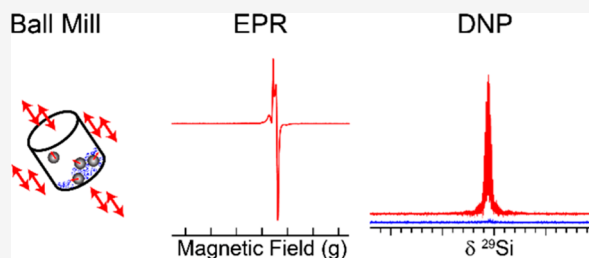


Article Recommendations



Supporting Information

ABSTRACT: High-field magic angle spinning (MAS) dynamic nuclear polarization (DNP) is becoming a common technique for improving the sensitivity of solid-state nuclear magnetic resonance (SSNMR) by the hyperpolarization of nuclear spins. Recently, we have shown that gamma irradiation is capable of creating long-lived free radicals that are amenable to MAS DNP in quartz and a variety of organic solids. Here, we demonstrate that ball milling is able to generate millimolar concentrations of stable radical species in diverse materials such as polystyrene, cellulose, borosilicate glass, and fused quartz. High-field electron paramagnetic resonance (EPR) was used to obtain further insight into the nature of the radicals formed in ball milled quartz and borosilicate glass. We further show that radicals generated in quartz by ball milling can be used for solid-effect DNP. We obtained ^{29}Si DNP enhancements of approximately 114 and 33 at 110 K and room temperature, respectively, from a sample of ball milled quartz.



INTRODUCTION

Nuclear magnetic resonance (NMR) spectroscopy is one of the most important techniques for probing structural information in disordered solids such as polymers^{1,2} and glasses.^{3–6} Unfortunately, NMR experiments on bulk inorganic solids often suffer from low sensitivity because nuclei such as ^{29}Si , ^{77}Se , ^{119}Sn , etc., have low natural isotopic abundance (<20%) and lengthy longitudinal relaxation times (T_1). In organic materials such as polymers cross-polarization (CP) from nearby ^1H spins is commonly used to increase NMR sensitivity of ^{13}C by enhancing the nuclear spin polarization and exploiting the T_1 of the ^1H spins to reduce the necessary relaxation delay.⁷ However, in many inorganic materials, there are often no ^1H spins present in the bulk to be used for CP.

Magic angle spinning (MAS) dynamic nuclear polarization (DNP) NMR spectroscopy is an emerging technique to improve the sensitivity of solid-state NMR experiments on a variety of inorganic materials.^{8–20} MAS DNP has found incredible success in the fields of nanoparticle and surface characterization.^{21–25} However, DNP requires the presence of a stable unpaired electron, typically provided by the addition of a nitroxide radical (TEKPOL, TOTAPOL, AMUPOL, bTbk, etc.) dissolved in a solvent (TCE, water/glycerol). Normally the ^1H spins in the solvent or at the surface of a material are hyperpolarized by DNP, with subsequent CP or other pulsed NMR techniques used to transfer polarization from ^1H spins to

hetero-nuclei that reside in surface species.^{10,22,24,26–28} Recently, Bjorgvinsdottir et al. have shown that it is possible to transfer magnetization from the surface to the bulk by incorporating long delays where slow nuclear spin diffusion can transport DNP-enhanced polarization from the surface into the bulk.^{12,14,29} Using this method, they were able to hyperpolarize moderately abundant nuclear spins residing in the bulk of tin oxide, lithium titanate, GaP, CdTe, and quartz. Some authors of the present work have also utilized this method to polarize ^{113}Cd and ^{77}Se spins found in the cores of CdS and CdSe quantum dots.^{30,31} However, the rate of nuclear spin diffusion in a given material and the longitudinal relaxation of the nuclear spins ultimately limits the achievable DNP enhancements.

In order to efficiently polarize nuclear spins residing in the bulk of a material it would be desirable to have a homogeneous distribution of radicals throughout the material. EPR-active metal dopants (Gd, Mn, Fe, etc.) at low concentrations have been shown to provide DNP enhancements in glasses,

Received: January 11, 2024

Revised: April 9, 2024

Accepted: April 10, 2024

Published: April 25, 2024



organometallic compounds, inorganic oxides, and proteins.^{15,17,19,32–36} Some materials, such as lithium batteries¹⁶ or silicon wafers,¹³ have intrinsic paramagnetic radical defects that have been used for DNP. Recently, our group has shown that ionizing radiation generates stable radicals that are compatible with MAS DNP in quartz and a variety of organic solids.^{37,38} Room-temperature DNP experiments were accessible for γ -irradiated quartz, glucose, malic acid, and maleic acid.^{37,38} However, access to γ -irradiation is often limited and/or expensive. Furthermore, the types of radicals created by γ -irradiation may not be suitable for high-field DNP.

Ball milling is known to create radicals in polymers at low temperatures and in an inert gas atmosphere.³⁹ We note that compressive forces have also been shown to create radicals in both synthetic and natural polymers.^{40–42} Mechanochemical processing of solids has recently found numerous applications in organic and inorganic synthesis,^{43–51} particle size adjustment,⁵² isotopic enrichment,^{53–55} preparation of multicomponent pharmaceuticals,^{56–62} catalysis,^{63–66} and other areas of solid-state chemistry and materials science.^{67–69} The wide variety of possible mechanochemistry applications and its simplicity make it appealing. Furthermore, since mechanochemistry uses minimal or no solvents, it is often more environmentally friendly than traditional solution-phase reactions.

Here, we demonstrate that mechanochemical treatment of quartz, borosilicate glass, cellulose, and other materials generates long-lived, air-stable radicals. These radicals are easily detected and quantified by room-temperature EPR spectroscopy. EPR spectroscopy is used to compare the radicals generated by mechanochemical methods and γ -irradiation for quartz, cellulose, and borosilicate glasses. Remarkably, the radical species created in the ball milled borosilicate glass and cellulose differ from those created by γ -irradiation, suggesting the ability to modify the radical species on the basis of the radical generation technique. The radical defects created by ball milling enable MAS DNP at both 100 K and room temperature for quartz.

METHODS

Samples. GE214 fused quartz tubing (10 mm \times 12 mm, ID \times OD) was purchased from GM Associates, Inc. The borosilicate glass was a 20 mL scintillation vial from Fisher Scientific. Cellulose was purchased from Aldrich; 290 kDa polystyrene was purchased from Alfa Aesar. Materials and synthesis for the NAPSO glass are described in refs 82 and 83. Preparation of TMDC materials followed the procedures given in ref 75.

Ionic Conductivity Measurements. The ionic conductivity of the mixed oxy-sulfide (MOS) NPSO melt-quench (MQ) and ball milled (BM) glassy solid-state electrolytes (GSEs) were measured using a Novocontrol 2 Dielectric spectrometer equipped with a cryostat capable of variable temperature impedance spectroscopy (IS) measurements between -100 and 300 °C (± 0.5 °C). Samples were measured using a custom, airtight sample holder to prevent unwanted reactions with O_2 or H_2O during the measurements. The complex impedance of the samples was measured from 3 MHz to 0.1 Hz at temperatures ranging from -10 to 150 °C. The ionic conductivity was determined by fitting the complex IS plot using the three-component equivalent circuit model described above. The temperature dependent resistance was

extracted from the fitted circuit model; the temperature dependent ionic conductivity was calculated.

Ball Milling Procedure and Setup. Samples were milled in a shaker mill (SPEX 8000 M Mixer/Mill) or a planetary mill (Fritsch, Pulverisette 7). Milling conditions are summarized in Table S1. About 2 g of sample was added to the milling jars unless otherwise noted. The borosilicate glass, cellulose, and polystyrene were milled in a 65 mL stainless steel jar with eight 11.9 mm diameter steel balls using a shaker mill with 1080 cycles per minute (Figure 1). Some materials were also milled

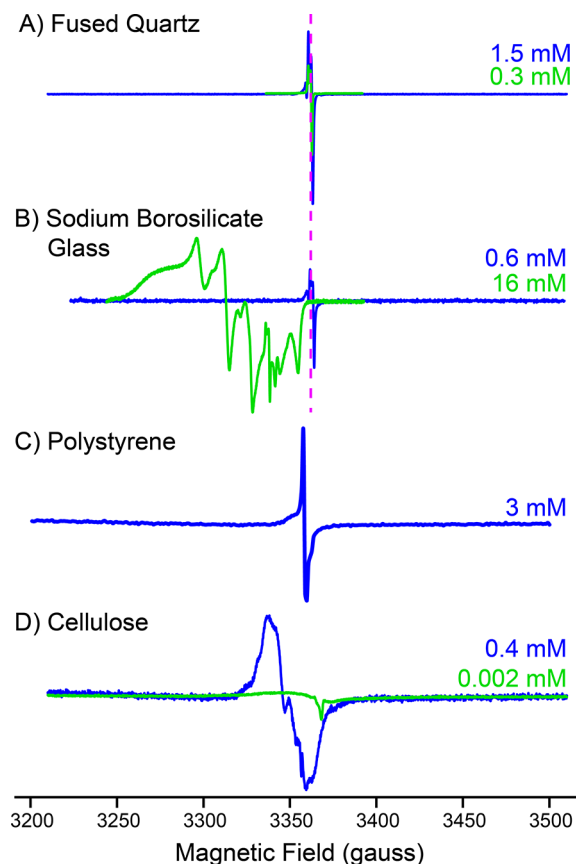


Figure 1. Room temperature X-band CW EPR spectra of ball milled (blue) and γ -irradiated (green) (A) fused quartz, (B) sodium borosilicate glass from a scintillation vial, (C) polystyrene, and (D) cellulose. Approximate solution equivalent concentrations of the free radicals are indicated. The vertical dashed line indicates the position of the E' radical. Quartz was milled in a planetary mill, while all other materials were milled in a shaker mill. Milling conditions are summarized in Table S1.

using a 45 mL zirconia jar with four 15 mm diameter zirconia balls in a planetary mill at 600 rpm (Figure S1). Within the shaker mill, the borosilicate glass and cellulose were milled for 1 h, and polystyrene was milled for 12 h (Figure 1). Quartz was milled with a planetary mill and a 45 mL zirconia vial with four 15 mm diameter zirconia balls at 600 rpm with milling durations of 0.5–4 h (Figure 1 and Table S2). Additional milling experiments on quartz were performed with a shaker mill using a 65 mL stainless steel jar with eight 11.9 mm diameter steel balls and a frequency of 1080 cycles per minute (Figure S1). We also tested grinding of quartz by hand in a mortar and pestle (Figure S1). The crystalline organic molecules (glucose, histidine hydrochloride monohydrate, malic acid, and salicylic acid) were milled for 30 min at

1080 cycles per minute in a 2.5 mL stainless-steel milling jar with one 6.35 mm diameter stainless-steel ball with a SPEX 8000 M Mixer/Mill (Figure S2). In these experiments approximately 0.1 g of each crystalline organic solid was loaded into the milling jar. Additional experiments were performed where approximately 2 g of glucose was milled for 1 h using a 45 mL zirconia jar with four 15 mm diameter zirconia balls in a planetary mill at 600 rpm (Figure S3). To synthesize $\text{MoWS}_{0.5}\text{Se}_{0.5}$, stoichiometric amounts of MoS_2 and WSe_2 (total mass of approximately 2 g) were combined in a 45 mL zirconia jar with four 15 mm diameter zirconia balls and ground in a planetary mill at 600 rpm for 30 h.

Dynamic Nuclear Polarization NMR. MAS DNP solid-state NMR spectroscopy experiments were performed on a commercial Bruker 263 GHz/400 MHz DNP system.⁷⁰ Sample temperatures of 110 K and room temperature were used for the experiments. ^{29}Si $\pi/2$ and π pulse durations of 4.0 μs and 8.0 μs were calibrated for 80 W of input power. ^{29}Si pulse durations were calibrated on an external sample of oxidized silicon nanocrystals impregnated with a 16 mM TEKPOL/TCE solution under DNP. Continuous wave 263 GHz microwaves with a power of ca. 30 W at the sample was used to saturate the electron spins for DNP transfer. The MAS frequency was 12500 Hz. ^{29}Si CPMG experiments were used to acquire the NMR spectra shown in Figures 5 and 6. Recycle delays between 100 and 20,000 s were used. Prior to acquisition of any NMR spectra, four “dummy” scans with a 1 s delay and 1 s of acquisition were used to saturate the ^{29}Si spins. In addition, 32 presaturation $\pi/2$ pulses separated by delays of 10 ms were applied before the recycle delay. 4200 CPMG loops were acquired, with each CPMG echo having a duration of 4.96 ms (62 rotor cycles). As discussed below, different numbers of echoes were used during processing to measure the DNP enhancements.

Electron Paramagnetic Resonance and Determination of Volumetric Radical Concentrations. Room temperature CW X-band EPR was performed on a Bruker ELEXSYS E580 system. Microwave attenuation was optimized for each sample. Radical concentrations were measured by first calibrating the response of the EPR spectrometer using an external standard consisting of a series of TEMPO in toluene solutions prepared by successive dilutions.³⁷ This standard was used to calibrate the equivalent volumetric radical concentration of powdered γ -irradiated quartz. The sample of γ -irradiated quartz was determined to have a concentration of free radicals that is equivalent to that of a 0.3 mM frozen TEMPO solution. Considering that the powdered materials are loosely packed into the EPR rotor, the true volumetric concentration of free radicals in the solid materials is likely higher. For each sample, the integrated intensity of the EPR spectrum was compared to that of γ -irradiated quartz to determine the equivalent volumetric concentration. The W-band measurements were performed using HiPER (High Power Electron Paramagnetic Spectrometer) located at the National High Magnetic Field Laboratory (NHMFL) in Tallahassee, Florida, using FEP plastic holders with sample volumes of 50 μL where fine powders of the different materials were placed.^{71–73} EPR was performed at 263 GHz and 100 K at the NHMFL using a homodyne high field spectrometer.⁷⁴

RESULTS AND DISCUSSION

Milling of Samples and Detection of Radicals by EPR Spectroscopy. First, we briefly describe why we chose to

study the various materials included in this paper. For several materials, we previously studied the formation of radicals induced by γ -irradiation (quartz, glucose, cellulose, borosilicate glasses).^{37,38} We also previously observed stable free radicals formed in milled samples of polystyrene.⁶⁶ Hence, these materials were all logical targets to investigate the creation of stable radicals by milling. Our interest in milled transition metal dichalcogenides (TMDCs) arose because Balema and co-workers have shown that ball milling of mixed TMDCs (i.e., MoS_2 and WSe_2) followed by annealing produced alloyed TMDCs which possess a homogeneous mixing of the transition metals and chalcogens.^{69,75} Ball milling of TMDCs and rare earth selenides was shown to create 3D heterostructure materials consisting of alternating TMDC layers and rare earth layers.^{69,75,76} Finally, we were interested in applying NMR to study the structure of the sodium thiophosphate (NaPSO) glasses as they have potential applications in battery materials as electrode spacers.⁷⁷ These materials are amorphous, and hence, their structure is often studied by NMR spectroscopy. One of the samples of NaPSO we studied was synthesized by mechanochemistry; hence, it is interesting to see if we can also observe free radicals in the as-synthesized material.

We begin with a demonstration that milling different materials produces long-lasting and air-stable radicals that are observable by continuous-wave, room-temperature X-band (9 GHz) electron paramagnetic resonance (EPR) spectroscopy. All samples were handled in air, and EPR measurements were also performed in air. Hence, in this study we are likely only observing stable, persistent radicals. The stable radical concentrations are measured by EPR (see the “Methods” section for further details). The radical concentrations are given in units of mM because the concentration of radicals in the solid materials was determined by comparing integrated intensities to a series of TEMPO solutions of a known volumetric concentration. Considering that the powdered materials are loosely packed into the EPR tubes, the true volumetric concentration of free radicals in the solid materials is likely higher. We note that the EPR spectra dramatically differ in appearance between the various milled materials, confirming that the observed EPR signals do not arise from metal particles or any other contamination from components of the mill.

Finally, it is important to note that EPR and DNP experiments were often performed days, weeks, and even months after milling, providing evidence for the long-term stability of the radical species. In the case of quartz, we performed EPR and DNP experiments several years after they were initially milled, again suggesting the high stability of some radicals formed by milling. For several materials we tested different milling conditions where we varied the type of container/milling media (steel vs zirconia) and the type of ball mill (shaker vs planetary). Changes in the achievable radical concentrations may occur due to aging or wear of the equipment used, but this point has not been investigated at this stage, as it is beyond the scope of the present study. Results from different milling conditions are summarized in Figures S1–S3 and Table S1 and are referred to below where appropriate.

Milling of Quartz and Sodium Borosilicate Glass. Milling was able to create significant concentrations of stable radicals in fused quartz glass and a sodium borosilicate glass (Figure 1). For amorphous quartz, we found that milling in a

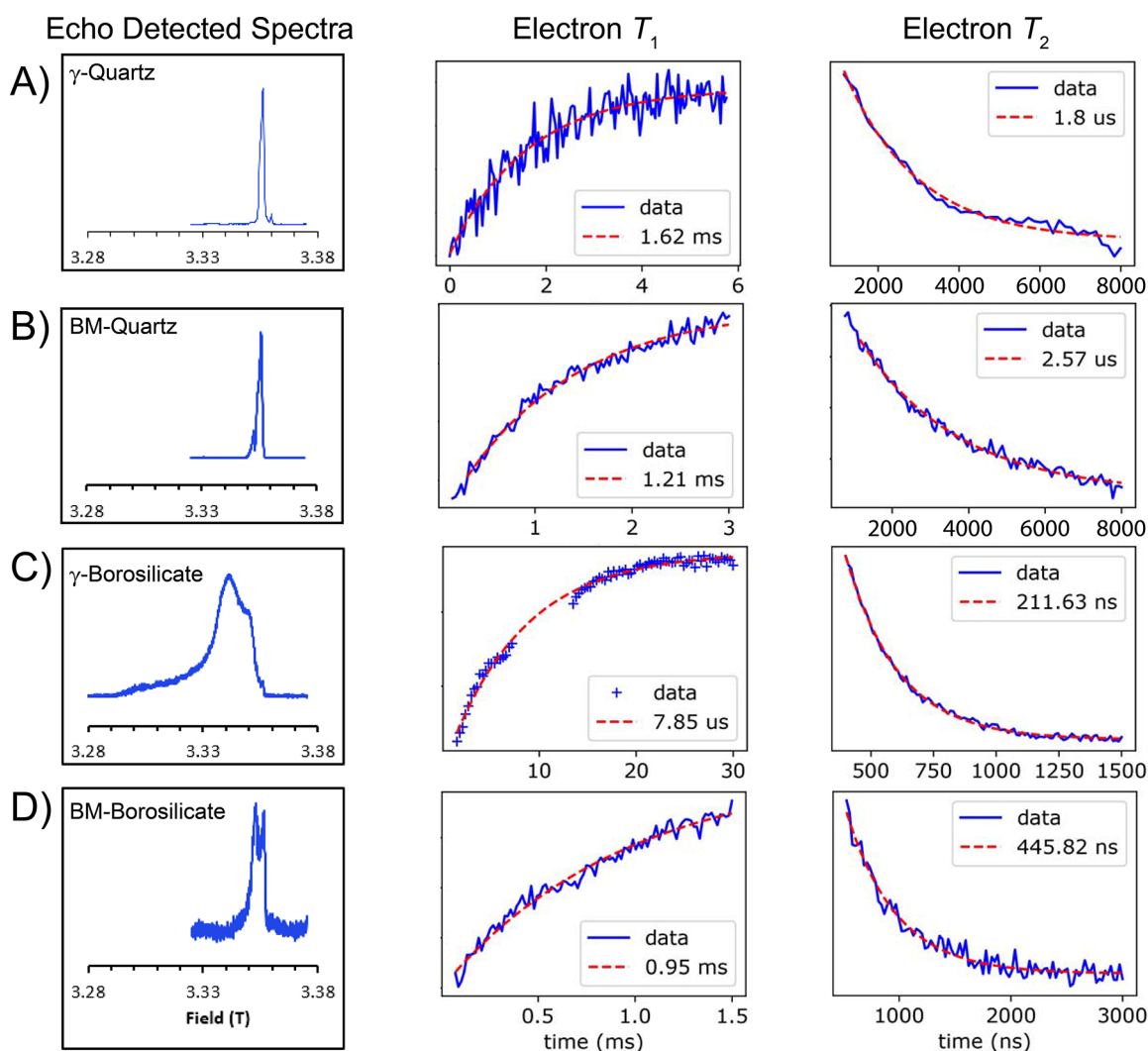


Figure 2. 100 K W-band EPR spectroscopy experiments on A) γ -irradiated quartz, B) ball milled quartz, C) γ -irradiated sodium borosilicate glass, and D) ball milled sodium borosilicate glass. (left) Echo detected EPR spectra, (middle) saturation recovery plots to measure electron T_1 , and (right) spin echo signal amplitudes to measure the electron T_2 . Note the differences in the x-axis ranges of the saturation recovery and transverse relaxation curves.

planetary mill with zirconia media gave the best results; milling in a shaker mill with steel media gave no observable radicals and resulted in significant contamination with steel (Figure S1 and Table S1). Both ball milling and γ -irradiation produce the silicon-centered oxygen vacancy (E') in quartz glass which is well studied in the literature (indicated by the dashed vertical line, Figure 1A,B).⁷⁸ An additional feature can be observed to the left (lower field) of the E' signal in the ball milled samples, which becomes more apparent when compared to γ -irradiated quartz (Figure S4). Attributing this site to any of the previously proposed stable radicals in quartz is difficult due to the inhomogeneous nature of fused quartz. There is a slight increase in the concentration of radicals created by ball milling, as opposed to γ -irradiation. The concentration of radicals formed in samples ball milled for 0.5, 1, and 4 h was approximately between 0.5 and 1.5 mM (Table S2).

For the borosilicate glass, the highest concentration of radicals were obtained when it was milled in a shaker mill with steel media. Akin to cellulose, ball milling of a sodium borosilicate glass results in drastically different EPR spectra as compared with the γ -irradiated borosilicate glass sample (Figure 1B and Figure S5). Based on the similarity of the

EPR spectra between ball milled borosilicate glass and ball milled or γ -irradiated quartz, we conclude that ball milling of the borosilicate glass forms a silicon-centered E' radical. On the other hand, the γ -irradiated borosilicate glass forms a nonbridging oxygen hole centered radical (NBOHC).^{37,79} In fact, boron-containing glasses are so sensitive to γ -rays that even minute amounts of boron in the sample lead to large concentrations of NBOHC radicals.⁷⁹ The broadening and splitting observed in the EPR spectrum of the γ -irradiated borosilicate glass arise because the NBOHC radicals exhibit significant hyperfine couplings to ^{10}B (NA = 19.9%) and ^{11}B (NA = 80.1%).

W-Band EPR Spectroscopy of Quartz and Sodium Borosilicate Glass. We measured the W-band (94 GHz) EPR spectra and the electron relaxation properties (T_{1e} and T_{2e} , see Table S3) to determine if these factors could explain the large differences in DNP enhancements realized for these materials (*vide infra*). The W-band EPR spectra were recorded at 100 K (Figure 2) and room temperature (Figure S6). The W-band EPR spectra confirm that similar concentrations and types of radicals were formed in ball milled and γ -irradiated quartz. Both ball milled and γ -irradiated quartz were found to have an

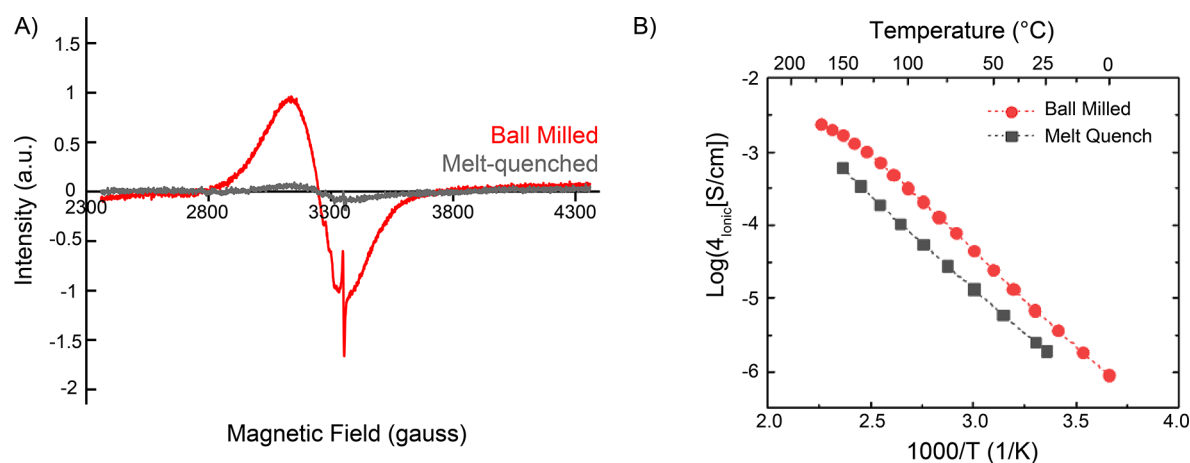


Figure 3. (A) X-band EPR spectra performed of NaPSO glass formed from ball milling (red) and melt-quench (gray) procedures. (B) Conductivity measurements on ball milled (red) and melt-quench (gray) NaPSO glass.

electron longitudinal relaxation time (T_{1e}) of more than 1 ms at 100 K, consistent with the values reported in a prior X-band EPR study of γ -irradiated quartz.⁷⁸ Note that the W-band spectra are direct absorption type spectra, while the X-band spectra are shown in derivative mode due to the nature of the measurement via field modulation. For γ -irradiated sodium borosilicate glass the W-band EPR spectrum shows an overall broad line with fewer features as compared to the X-band EPR spectrum (Figure 2C). This result is expected, as the g -anisotropy is likely larger than the ^{10}B and ^{11}B hyperfine splittings at the higher magnetic field. Lastly, the W-band spectrum of the ball milled borosilicate glass shows similar features as were seen in the quartz samples (Figure 2D). The visibly higher noise is indicative of lower radical concentration (0.6 mM) as compared to the other materials that possessed higher radical concentrations. Interestingly, the milled quartz and milled borosilicate glass had similar EPR spectra (*vide supra*) and showed similar T_{1e} values, but the electron transverse relaxation time (T_{2e}) of the borosilicate glass was about 1 order of magnitude smaller than the ball milled quartz. The short T_{2e} for the borosilicate glass likely occurs due to the presence of abundant boron and sodium spins in the glass (Table S3). EPR was also performed at 263 GHz and 100 K (Figure S7), the same field as 400 MHz DNP. Similar features are observed in the EPR spectra collected at W-band (94 GHz) and 263 GHz.

Milling of Polystyrene. Mechanically degraded polystyrene was previously shown to yield stable free radicals, although limited details were provided on their mechanical degradation procedure.⁸⁰ Previously, some of the coauthors of this paper have shown that ball milling of polystyrene leads to the formation of stable radicals and also causes depolymerization to styrene.⁶⁶ It was shown that it was crucial to use metallic milling media in order to obtain the highest concentration of free radicals.⁶⁶ Hence, we chose to use stainless-steel milling media for polystyrene, and we obtained a significant concentration of radicals (Figure 1C). Consistent with prior results, we also found that the use of zirconia milling media with a planetary mill gave a low concentration of free radicals (Figure S1). The radical species produced during milling of polystyrene are primarily thought to arise from carbon-centered radicals that reside on the carbon atoms of the polymer backbone.⁸⁰ The relatively narrow EPR signals observed here are consistent with the assignment to carbon-

centered radicals. We previously observed EPR spectra of milled polystyrene that showed narrow signals from carbon-centered radicals and broader signals with peak widths on the order of 1500 G that were attributed to peroxide radicals.⁶⁶ The broader peroxide radicals were not observed here, likely due to the smaller sweep width used to record the EPR spectrum.

Milling of Microcrystalline Cellulose. Microcrystalline cellulose is a polymer of glucose that has uses in sustainable materials, biofuels, and pharmaceuticals because it is readily obtained from plant biomass. It has previously been shown that ball milling of microcrystalline cellulose resulted in intense EPR signals.^{64,81} Here, we observe that the ball milling of cellulose in a shaker mill with steel media leads to a significant free radical concentration. Interestingly, the concentration of radicals obtained by milling is about 3 orders of magnitude higher than was obtained with a ca. 30 kGy dose of γ -irradiation (Figure 1D and Figure S8).³⁷ The breadth of the EPR spectrum varies significantly for ball milled cellulose (blue) and γ -irradiated cellulose (green), indicating that different radical species are present in the two separate samples. Thus, the technique used for creating radicals can be chosen to control the concentration and types of radicals that are formed. The EPR signals of the milled cellulose are much broader than those of polystyrene, consistent with literature assignments that milled cellulose primarily contains oxygen-centered radicals.⁸¹

Milling of NaPSO Glass. A sodium thiophosphate (“NaPSO”) glass which has potential applications as a solid-state electrolyte was prepared by two different methods: heating of the components to ca. 700 °C followed by rapid quenching⁸² and by ball milling the compounds together for 20 h in a Fritsch planetary mill.⁸³ We note that mechanochemistry is commonly used in the synthesis of inorganic glasses or for postsynthetic processing of glass materials. While the materials prepared by the two synthetic routes appeared structurally identical by Raman, FT-IR, and NMR spectroscopies, there was a drastic difference in the value of the conductivity measurement between the two samples, with the mechanochemically prepared sample having better conductivity by a factor of 5. EPR spectroscopy of the two samples indicated that the ball milled sample had an order of magnitude more radicals than did the sample prepared using the standard melt-quench procedure (Figure 3). We propose that the radicals formed in

the NaPSO glass during milling are sulfur- or oxygen-centered radicals because there is no clear hyperfine coupling (as would be in the case for radicals located near Na or P) and there is a large line width indicative of *g*-anisotropy.

Milling of Transition Metal Dichalcogenides. Significant concentrations of paramagnetic centers were also observed in ball milled TMDCs. Here, we prepared $\text{Mo}_{0.5}\text{W}_{0.5}\text{SSe}$ by milling MoS_2 and WSe_2 in a planetary-type mill. We first noticed the formation of radicals in milled TMDCs because we were attempting to perform MAS DNP experiments on $\text{Mo}_{0.5}\text{W}_{0.5}\text{SSe}$ by impregnating it with a nitroxide biradical tetrachloroethane solution.²⁶ However, we observed negligible ^1H DNP enhancements and a very long ^1H T_1 of ca. 100 s for the frozen tetrachloroethane. These observations led us to conclude that in the milled TMDC samples impregnated with nitroxide radicals, the nitroxides were likely destroyed by a reaction with paramagnetic species that were associated with the TMDC. Indeed, the X-band EPR spectrum of $\text{Mo}_{0.5}\text{W}_{0.5}\text{SSe}$ prepared by ball milling shows an intense set of signals (Figure 4A). We estimate that the total

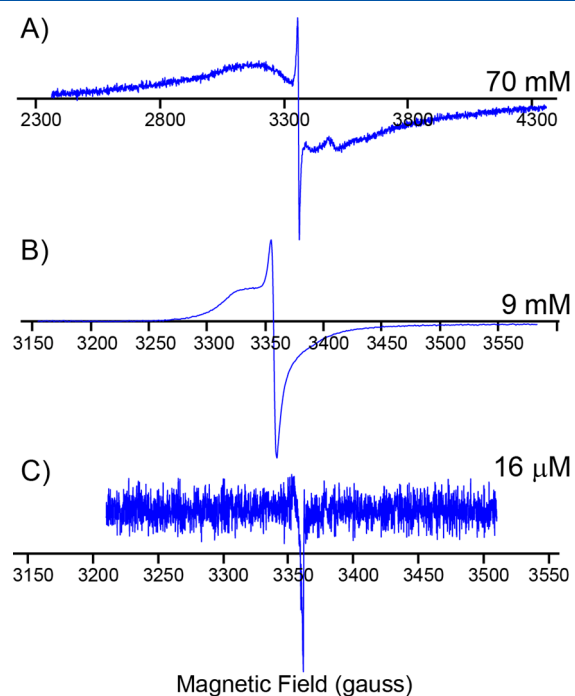


Figure 4. X-band EPR spectra of A) $\text{Mo}_{0.5}\text{W}_{0.5}\text{SSe}$ obtained by ball milling of WSe_2 and MoS_2 , B) $\text{Mo}_{0.5}\text{W}_{0.5}\text{SSe}$ ball milled and annealed, and C) as-received WSe_2 (not subjected to ball milling). Note the different magnetic field *x*-axis scales for the spectra (see Figure S9 for EPR spectra plotted on the same *x*-axis scale).

radical concentration present in the sample of $\text{Mo}_{0.5}\text{W}_{0.5}\text{SSe}$ prepared by milling was equivalent to that of a 70 mM TEMPO solution. One of the signals is very broad and likely corresponds to paramagnetic coordinatively unsaturated transition metal centers that reside at the edges of the TMDC sheets. The sharper signal is assigned to sulfur- or selenium-centered radicals. Unsaturated chalcogen and transition metal atoms associated with defects or edge sites are known to be present in TMDC materials.^{84–86} Nearly all of the broad EPR signal is removed upon annealing in a sealed quartz tube at 1000 °C for 16 h. The quartz tube was backfilled with a 0.75 bar helium atmosphere prior to sealing.⁷⁵ After annealing,

the narrower EPR signals remain with an estimated radical concentration of 9 mM (Figure 4B). This observation suggests that many of coordinatively unsaturated transition metal or chalcogens formed during milling likely recombine during the annealing process, although a significant fraction of the sulfur- or selenium-centered radicals survived the annealing process. We performed EPR on the as-received WSe_2 prior to ball-milling and observed a free radical concentration of only 16 μM (Figure 4C).

Milling of Molecular Organic Solids. As a control experiment, four microcrystalline organic solids (glucose, histidine hydrochloride monohydrate, malic acid, and salicylic acid) were ball milled. X-band EPR spectroscopy suggests there are insignificant concentrations of stable radicals in all of these milled solids (Figures S2 and S3). We also applied solution ^1H and ^{13}C NMR to confirm that milling does not lead to changes in the molecular structure or the formation of impurities when glucose is subjected to milling (Figure S10). The observation of low radical concentrations in the molecular solids was anticipated because intermolecular forces between organic molecules are much weaker than covalent bonds. Hence, milling will likely cause disorder and promote slippage of small molecules as opposed to the breakage of covalent chemical bonds that is observed when polymers or network materials are milled. Note that grinding and milling are well-known to reduce the ^1H T_1 of molecular organic solids.^{87–90} The reduction in ^1H T_1 has been hypothesized to arise from a reduction in the particle size or creation of amorphous domains.^{87–90}

MAS DNP Experiments on Milled Materials. Previously, we have shown that radicals formed during γ -irradiation of quartz and a variety of organic solids are amenable to MAS DNP.^{37,38} Here, we evaluated the suitability of the radicals generated through mechanochemical methods for MAS DNP. We performed MAS DNP NMR experiments on ball milled polystyrene, cellulose, borosilicate glass, and quartz glass (Figures 5 and S11–S16). However, only ball milled quartz gave observable DNP enhancements. DNP field sweeps were performed for all solids. For further discussion of the negative results, see below.

The optimal position of the magnetic field for solid effect DNP transfer for ball milled quartz was similar to that reported for γ -irradiated quartz (Figure 5A).³⁷ The ^{29}Si refocused transverse relaxation time (T_2') of quartz is so long that Carr–Purcell–Meiboom–Gill (CPMG) echoes were able to be acquired for more than 20 s (Figure S17); further acquisition of the FID was limited by the memory capacity of the spectrometer. While the ^{29}Si T_1 of the amorphous quartz is greater than 19 h at 110 K,³⁷ CPMG provides a significant boost in sensitivity enabling observation of the ^{29}Si NMR signal with acquisition of only a single scan. DNP experiments were performed on quartz that was ball milled for three different lengths of time: 0.5, 1, and 4 h. The quartz subjected to 1 h of milling provided the best DNP enhancement of 114, but significant enhancements of 78 and 23 were obtained for the 0.5 and 4 h milled samples, respectively (Figure S11). These enhancements were all measured with 10,000 s recycle delays. The measured enhancement depends upon the recycle delay that is chosen (Figure S11). Comparison of enhancements for the different samples shows that the duration of milling should be optimized so that milling generates enough radicals for DNP, while at the same time avoiding excessive

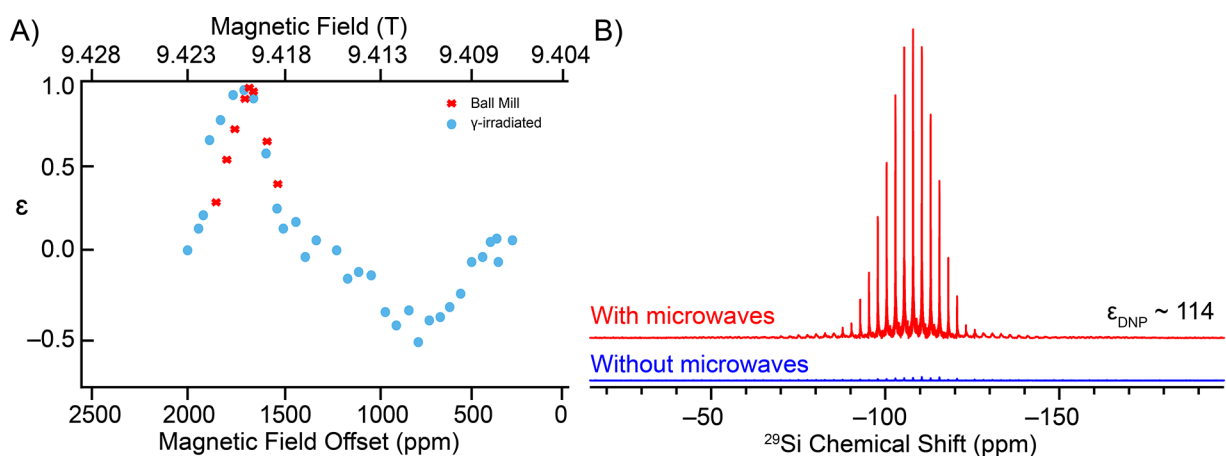


Figure 5. (A) Comparison of ^{29}Si DNP field sweep profiles for ball milled (red crosses) and γ -irradiated (blue circles) quartz. DNP enhancements of the field sweeps are normalized to better compare offset. (B) ^{29}Si CPMG MAS solid-state NMR spectra obtained without and with microwaves. The main magnetic field was set to maximize DNP. A single scan was acquired. The first 160 ms of the CPMG echo train was used in the Fourier transform. The sample temperature was ca. 110 K for all of these experiments. The quartz was milled for 1 h in a planetary mill.

milling that leads to agglomeration of the small particles, as is known to happen during the milling process.⁹¹

There is one caution for the measurement of ^{29}Si DNP enhancements for quartz. The measured DNP enhancements strongly depend upon the number of CPMG echoes used in processing. The enhancements indicated in Figures 5 and 6

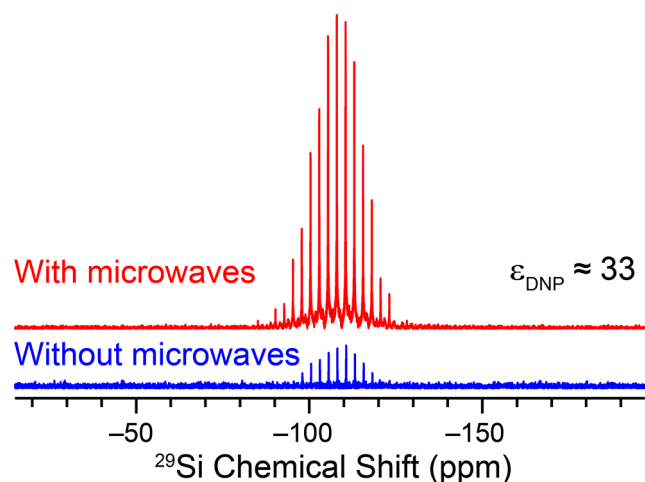


Figure 6. Room temperature MAS DNP NMR ^{29}Si CPMG NMR spectra of quartz that was ground in a planetary mill for 1 h. 1 and 4 scans were used to acquire the NMR spectra with and without microwaves, respectively. The recycle delay was 10,000 s.

were measured by Fourier transform of the echoes in the first 160 ms of the CPMG echo train (33 echoes). If instead echoes in the first 5 s of the CPMG echo train (1008 echoes) are included in the Fourier transform, then there is a significant drop in the DNP enhancement from 114 to 55 (Figure S18). Using the full CPMG echo train (4200 echoes, 20.832 s) in the Fourier transform results in a DNP enhancement of 32. The drop in enhancement with increasing CPMG FID likely occurs because ^{29}Si spins that are closest to the radicals will have larger DNP enhancements, but these same spins will also have shorter ^{29}Si T_2' . On the other hand, the spectrum recorded without DNP gives higher relative weighting to ^{29}Si spins that are further on average from the radicals, which will have a longer T_2' .

DNP is typically limited to low temperatures of 110 K or less due to the T_{1e} of the radical. However, MAS at low temperatures poses several challenges along with the added cost of cryogenics. In addition, samples may change phase or crystal structures by going from 300 to 100 K. For all of these reasons, there are many potential advantages to performing DNP at room temperature. Due to the prior success of room temperature DNP experiments on γ -irradiated quartz,³⁷ we attempted DNP experiments on the ball milled quartz at room temperature (Figure 6). DNP enhancements were ca. 33, about a quarter of the enhancement realized at 110 K. If the full CPMG echo train is used for the Fourier transform, then an enhancement of 4 was obtained. Sizable DNP enhancements are obtained at room temperature due to the abnormally long ^{29}Si T_1 and electron T_1 of the E' center of quartz. Prior X-band EPR experiments indicated the T_{1e} of γ -irradiated quartz was approximately 300 μs at 220 K.⁷⁸ Room temperature W-band EPR measurements for ball milled quartz at room temperature gave T_{1e} and T_{2e} values of 223 μs and 4 μs , respectively (Table S3 and Figure S6). The room temperature T_{1e} of ball milled or γ -irradiated quartz is longer than the T_{1e} of standard nitroxide radicals at 100 K (ca. 50 μs).^{92,93}

We note that while the concentration of radicals is higher in ball milled quartz than in γ -irradiated quartz, but, lower DNP enhancements were achieved with the ball milled material. It is well-known that γ -rays can easily penetrate most materials; hence, radical defects created by γ -irradiation should be homogeneously distributed throughout the material. We hypothesize that the radicals produced by milling are most likely concentrated near the edges of grain boundaries, where covalent bonds have been cleaved during the milling process. In the ball milled samples, the radicals are likely heterogeneously distributed, with an increased concentration toward the surface or edges of the particles. This hypothesis could explain why low or no DNP enhancement was obtained for several samples, despite the sizable concentration of radicals created by milling.

Radical clustering might explain the lack of DNP enhancements in ball milled cellulose and polystyrene. From the EPR spectrum alone, both cellulose and polystyrene appear to be ideal for DNP because they have intense and relatively narrow EPR signals and a sizable concentration of free radicals.

However, DNP was ultimately unsuccessful, either due to an inhomogeneous distribution of radicals or unfavorable electronic or nuclear relaxation properties. We note that for polystyrene a short ^1H T_1 on the order of 8 s was observed, even after degassing (to remove dissolved O_2). The ^1H T_1 of 8 s would prevent accumulation of ^1H spin polarization and could also explain why the DNP failed here. It would be interesting to perform DNP experiments at liquid helium sample temperatures to see if the ^1H T_1 could be prolonged and if that would allow DNP to work. No DNP enhancements could be realized for the ball milled borosilicate glass, despite its EPR spectrum being very similar to that of quartz. In addition, DNP experiments on the borosilicate glass will be hindered by the abundant quadrupolar spins in the material (e.g., ^{11}B , ^{23}Na , ^{27}Al). The quadrupolar spins will likely act as polarization sinks because of their high abundance and short T_1 relaxation times. When the field position is optimized to polarize ^{29}Si , there would still be significant polarization transfer to the quadrupolar spins which are close in Larmor frequency to ^{29}Si . We note that the radicals in the borosilicate glass also showed reduced T_{2e} as compared to that in quartz (Table S3), and a shorter T_{2e} will also be detrimental to DNP.

CONCLUSIONS

Mechanochemical processing of inorganic and organic network solids generates persistent radicals. We did not observe the formation of significant concentrations of stable radicals when microcrystalline molecules were milled. For cellulose and borosilicate glass, the radical that is formed by milling is of a different chemical structure than that formed by γ -irradiation, indicating that milling could be complementary to γ -irradiation because it can create different types of free radicals in some cases. There was a significant concentration of radicals produced in ball milled polystyrene, cellulose, borosilicate glass, and fused quartz. However, only the radicals in ball milled quartz were able to be used for MAS DNP. We suspect that unfavorable nuclear relaxation times prevented DNP enhancements from being observed in many of these other systems. The DNP enhancement of ball milled quartz was 114 at 110 K, which reduces the measurement times of NMR experiments on quartz by about 4 orders of magnitude. Further, room temperature DNP experiments of ball milled quartz resulted in DNP enhancements of ca. 33. It is possible that ionizing radiation methods in combination with ball milling could create some interesting and useful radicals for the MAS DNP. More research into the paramagnetic centers and free radicals created by ball milling is needed. EPR spectroscopy should be used to obtain insights into the properties of the radicals formed and to probe the underlying DNP mechanisms. We anticipate that future pulsed MAS DNP methods could be utilized to realize DNP enhancements in some of these materials, especially ball-milled borosilicate glass. Lower temperature DNP experiments using helium cooled samples could also be beneficial, as lower temperatures generally prolong nuclear and electronic relaxation time constants.

ASSOCIATED CONTENT

Supporting Information

The Supporting Information is available free of charge at <https://pubs.acs.org/doi/10.1021/acs.jpca.4c00228>.

Additional X-band, W-band, and 263 GHz EPR spectra and concentrations, MAS DNP data, and solution NMR data (PDF)

AUTHOR INFORMATION

Corresponding Authors

Aaron J. Rossini – U.S. Department of Energy, Ames National Laboratory, Ames, Iowa 50011, United States; Iowa State University, Department of Chemistry, Ames, Iowa 50011, United States; orcid.org/0000-0002-1679-9203; Phone: +1-515-294-8952; Email: arossini@iastate.edu

Scott L. Carnahan – U.S. Department of Energy, Ames National Laboratory, Ames, Iowa 50011, United States; Iowa State University, Department of Chemistry, Ames, Iowa 50011, United States; St. Mary's University of Minnesota, Department of Chemistry, Winona, Minnesota 55987, United States; orcid.org/0000-0001-8063-6102; Phone: +1-507-457-1556; Email: scarnaha@smumn.edu

Authors

Kipper Riemersma – Iowa State University, Department of Chemistry, Ames, Iowa 50011, United States

Ihor Z. Hlova – U.S. Department of Energy, Ames National Laboratory, Ames, Iowa 50011, United States; orcid.org/0000-0002-7620-9957

Oleksandr Dolotko – U.S. Department of Energy, Ames National Laboratory, Ames, Iowa 50011, United States

Steven J. Kmiec – Iowa State University, Department of Materials Science and Engineering, Ames, Iowa 50011, United States

Sujeewa N. S. Lamahewage – U.S. Department of Energy, Ames National Laboratory, Ames, Iowa 50011, United States; Iowa State University, Department of Chemistry, Ames, Iowa 50011, United States

Steve W. Martin – Iowa State University, Department of Materials Science and Engineering, Ames, Iowa 50011, United States; orcid.org/0000-0002-6472-509X

James F. Wishart – Chemistry Division, Brookhaven National Laboratory, Upton, New York 11973, United States; orcid.org/0000-0002-0488-7636

Thierry Dubroca – National High Magnetic Field Laboratory, Tallahassee, Florida 32310, United States

Viktor P. Balema – U.S. Department of Energy, Ames National Laboratory, Ames, Iowa 50011, United States; Clemson University, Materials Science & Engineering, Clemson, South Carolina 29634, United States

Complete contact information is available at: <https://pubs.acs.org/10.1021/acs.jpca.4c00228>

Notes

The authors declare no competing financial interest.

ACKNOWLEDGMENTS

We acknowledge Prof. Javier Vela for the use of his shaker mill. DNP-enhanced solid-state NMR experiments, EPR experiments, and data analysis (S.L.C., K.R., S.N.S.L., and A.J.R.) were supported by the U.S. Department of Energy (DOE), Office of Science, Basic Energy Sciences, Materials Science and Engineering Division. The Ames National Laboratory is operated for the U.S. DOE by Iowa State University under Contract DE-AC02-07CH11358. NaPSO glass synthesis and characterization (S.J.K and S.W.M) were supported by the

Department of Energy Vehicular Technologies Office, Energy Storage Contract DE-EE-0008852, and Pacific Northwest National Laboratory and Battelle Memorial Institute SubContract number 679315. Part of this work was performed at the National High Magnetic Field Laboratory, which is supported by the National Science Foundation (NSF) cooperative agreement numbers DMR-1644779 and DMR-2128556 and the state of Florida. γ -irradiation experiments (J.F.W.) were supported by the U.S. Department of Energy (DOE), Office of Science, Basic Energy Sciences, Chemical Sciences, Biosciences and Geosciences Division under contract DE-SC0012704 with Brookhaven National Laboratory.

REFERENCES

- (1) Schmidt-Rohr, K.; Spiess, H. W. *Multidimensional Solid-State NMR and Polymers*; Academic Press Inc., 1994.
- (2) Brown, S. P.; Spiess, H. W. *Advanced Solid-State NMR Methods for the Elucidation of Structure and Dynamics of Molecular, Macromolecular, and Supramolecular Systems*. *Chem. Rev.* **2001**, *101* (12), 4125–56.
- (3) Eckert, H. Structural Characterization of Noncrystalline Solids and Glasses Using Solid State NMR. *Prog. Nucl. Magn. Reson. Spectrosc.* **1992**, *24*, 159–293.
- (4) Eckert, H. Structural Characterization of Bioactive Glasses by Solid State NMR. *J. Sol-Gel Sci. Technol.* **2018**, *88* (2), 263–295.
- (5) Youngman, R. NMR Spectroscopy in Glass Science: A Review of the Elements. *Materials (Basel)*. **2018**, *11* (4), 476 Mar 22.
- (6) Tricot, G.; Alpyssbay, L.; Doumert, B. Solid State NMR: A Powerful Tool for the Characterization of Borophosphate Glasses. *Molecules* **2020**, *25*, 428.
- (7) Pines, A.; Gibby, M. G.; Waugh, J. S. Proton-Enhanced NMR of Dilute Spins in Solids. *J. Chem. Phys.* **1973**, *59* (2), 569–590.
- (8) Maly, T.; Debelouchina, G. T.; Bajaj, V. S.; Hu, K.-N.; Joo, C.-G.; Mak-Jurkauskas, M. L.; Sirigiri, J. R.; van der Wel, P. C. A.; Herzfeld, J.; Temkin, R. J.; Griffin, R. G. Dynamic Nuclear Polarization at High Magnetic Fields. *J. Chem. Phys.* **2008**, *128* (5), 052211.
- (9) Hope, M. A.; Halat, D. M.; Magusin, P. C.; Paul, S.; Peng, L.; Grey, C. P. Surface-Selective Direct ^{17}O DNP NMR of CeO_2 Nanoparticles. *Chem. Commun.* **2017**, *53* (13), 2142–2145.
- (10) Liao, W. C.; Ong, T. C.; Gajan, D.; Bernada, F.; Sauvee, C.; Yulikov, M.; Pucino, M.; Schowner, R.; Schwarzwald, M.; Buchmeiser, M. R.; et al. Dendritic Polarizing Agents for DNP SENS. *Chem. Sci.* **2017**, *8* (1), 416–422.
- (11) Lilly Thankamony, A. S.; Wittmann, J. J.; Kaushik, M.; Corzilius, B. Dynamic Nuclear Polarization for Sensitivity Enhancement in Modern Solid-State NMR. *Prog. Nucl. Magn. Reson. Spectrosc.* **2017**, *102–103*, 120–195.
- (12) Bjorgvinsdottir, S.; Walder, B. J.; Pinon, A. C.; Emsley, L. Bulk Nuclear Hyperpolarization of Inorganic Solids By Relay From the Surface. *J. Am. Chem. Soc.* **2018**, *140* (25), 7946–7951.
- (13) Ha, M.; Thiessen, A. N.; Sergeev, I. V.; Veinot, J. G. C.; Michaelis, V. K. Endogenous Dynamic Nuclear Polarization NMR of Hydride-Terminated Silicon Nanoparticles. *Solid State Nucl. Magn. Reson.* **2019**, *100*, 77–84.
- (14) Bjorgvinsdottir, S.; Moutzouri, P.; Berruyer, P.; Hope, M. A.; Emsley, L. Sensitivity Enhancements in Lithium Titanates by Incipient Wetness Impregnation DNP NMR. *J. Phys. Chem. C* **2020**, *124* (30), 16524–16528.
- (15) Harchol, A.; Reuveni, G.; Ri, V.; Thomas, B.; Carmieli, R.; Herber, R. H.; Kim, C.; Leskes, M. Endogenous Dynamic Nuclear Polarization for Sensitivity Enhancement in Solid-State NMR of Electrode Materials. *J. Phys. Chem. C Nanomater Interfaces* **2020**, *124* (13), 7082–7090.
- (16) Hope, M. A.; Rinkel, B. L. D.; Gunnarsdottir, A. B.; Marker, K.; Menkin, S.; Paul, S.; Sergeev, I. V.; Grey, C. P. Selective NMR Observation of the SEI-Metal Interface by Dynamic Nuclear Polarisation from Lithium Metal. *Nat. Commun.* **2020**, *11* (1), 2224.
- (17) Jardon-Alvarez, D.; Reuveni, G.; Harchol, A.; Leskes, M. Enabling Natural Abundance ^{17}O Solid-State NMR by Direct Polarization from Paramagnetic Metal Ions. *J. Phys. Chem. Lett.* **2020**, *11* (14), 5439–5445.
- (18) Paterson, A. L.; Perras, F. A.; Besser, M. F.; Pruski, M. Dynamic Nuclear Polarization of Metal-Doped Oxide Glasses: A Test of the Generality of Paramagnetic Metal Polarizing Agents. *J. Phys. Chem. C* **2020**, *124* (42), 23126–23133.
- (19) Jardon-Alvarez, D.; Kahn, N.; Houben, L.; Leskes, M. Oxygen Vacancy Distribution in Yttrium-Doped Ceria from $(89)\text{Y}$ - $(89)\text{Y}$ Correlations via Dynamic Nuclear Polarization Solid-State NMR. *J. Phys. Chem. Lett.* **2021**, *12* (11), 2964–2969.
- (20) Rossini, A. J. Materials Characterization by Dynamic Nuclear Polarization-Enhanced Solid-State NMR Spectroscopy. *J. Phys. Chem. Lett.* **2018**, *9* (17), 5150–5159.
- (21) Lesage, A.; Lelli, M.; Gajan, D.; Caporini, M. A.; Vitzthum, V.; Mieville, P.; Alauzun, J.; Roussey, A.; Thieuleux, C.; Mehdi, A.; et al. Surface Enhanced NMR Spectroscopy by Dynamic Nuclear Polarization. *J. Am. Chem. Soc.* **2010**, *132*, 15459–15461.
- (22) Rossini, A. J.; Zagdoun, A.; Lelli, M.; Lesage, A.; Coperet, C.; Emsley, L. Dynamic Nuclear Polarization Surface Enhanced NMR Spectroscopy. *Acc. Chem. Res.* **2013**, *46* (9), 1942–51.
- (23) Perras, F. A.; Kobayashi, T.; Pruski, M. Natural Abundance ^{17}O DNP Two-Dimensional and Surface-Enhanced NMR Spectroscopy. *J. Am. Chem. Soc.* **2015**, *137* (26), 8336–8339.
- (24) Pump, E.; Viger-Gravel, J.; Abou-Hamad, E.; Samantaray, M. K.; Hamzaoui, B.; Gurinov, A.; Anjum, D. H.; Gajan, D.; Lesage, A.; Bendjeriou-Sedjerari, A.; et al. Reactive Surface Organometallic Complexes Observed Using Dynamic Nuclear Polarization Surface Enhanced NMR Spectroscopy. *Chem. Sci.* **2017**, *8* (1), 284–290.
- (25) Li, W.; Wang, Q.; Xu, J.; Aussenac, F.; Qi, G.; Zhao, X.; Gao, P.; Wang, C.; Deng, F. Probing the Surface of $\gamma\text{-Al}_2\text{O}_3$ by Oxygen-17 Dynamic Nuclear Polarization Enhanced Solid-State NMR Spectroscopy. *Phys. Chem. Chem. Phys.* **2018**, *20*, 17218–17225.
- (26) Lesage, A.; Lelli, M.; Gajan, D.; Caporini, M. A.; Vitzthum, V.; Mieville, P.; Alauzun, J.; Roussey, A.; Thieuleux, C.; Mehdi, A.; et al. Surface Enhanced NMR Spectroscopy by Dynamic Nuclear Polarization. *J. Am. Chem. Soc.* **2010**, *132* (44), 15459–61.
- (27) Perras, F. A.; Wang, L.; Manzano, J. S.; Chaudhary, U.; Opembe, N. N.; Johnson, D. D.; Slowing, I. I.; Pruski, M. Optimal Sample Formulations for DNP SENS: The Importance of Radical-Surface Interactions. *Curr. Opin. Colloid Interface Sci.* **2018**, *33*, 9–18.
- (28) Nagashima, H.; Trebosc, J.; Kon, Y.; Sato, K.; Lafon, O.; Amoureux, J. P. Observation of Low-gamma Quadrupolar Nuclei by Surface-Enhanced NMR Spectroscopy. *J. Am. Chem. Soc.* **2020**, *142* (24), 10659–10672.
- (29) Bjorgvinsdottir, S.; Walder, B. J.; Matthey, N.; Emsley, L. Maximizing Nuclear Hyperpolarization in Pulse Cooling under MAS. *J. Magn. Reson.* **2019**, *300*, 142–148.
- (30) Hanrahan, M. P.; Chen, Y.; Blome-Fernandez, R.; Stein, J. L.; Pach, G. F.; Adamson, M. A. S.; Neale, N. R.; Cossairt, B. M.; Vela, J.; Rossini, A. J. Probing the Surface Structure of Semiconductor Nanoparticles by DNP SENS with Dielectric Support Materials. *J. Am. Chem. Soc.* **2019**, *141* (39), 15532–15546.
- (31) Chen, Y.; Dorn, R. W.; Hanrahan, M. P.; Wei, L.; Blome-Fernandez, R.; Medina-Gonzalez, A. M.; Adamson, M. A. S.; Flintgruber, A. H.; Vela, J.; Rossini, A. J. Revealing the Surface Structure of CdSe Nanocrystals by Dynamic Nuclear Polarization-Enhanced $(77)\text{Se}$ and $(113)\text{Cd}$ Solid-State NMR Spectroscopy. *J. Am. Chem. Soc.* **2021**, *143* (23), 8747–8760.
- (32) Corzilius, B.; Smith, A. A.; Barnes, A. B.; Luchinat, C.; Bertini, I.; Griffin, R. G. High-Field Dynamic Nuclear Polarization With High-Spin Transition Metal Ions. *J. Am. Chem. Soc.* **2011**, *133* (15), 5648–51.
- (33) Corzilius, B.; Michaelis, V. K.; Penzel, S. A.; Ravera, E.; Smith, A. A.; Luchinat, C.; Griffin, R. G. Dynamic Nuclear Polarization of ^1H , ^{13}C , and ^{59}Co in a Tris(ethylenediamine)cobalt(III) Crystalline

- Lattice Doped with Cr(III). *J. Am. Chem. Soc.* **2014**, *136* (33), 11716–27.
- (34) Kaushik, M.; Bahrenberg, T.; Can, T. V.; Caporini, M. A.; Silvers, R.; Heiliger, J.; Smith, A. A.; Schwalbe, H.; Griffin, R. G.; Corzilius, B. Gd(III) and Mn(II) Complexes for Dynamic Nuclear Polarization: Small Molecular Chelate Polarizing Agents and Applications with Site-Directed Spin Labeling of Proteins. *Phys. Chem. Chem. Phys.* **2016**, *18* (39), 27205–27218.
- (35) Chakrabarty, T.; Goldin, N.; Feintuch, A.; Houben, L.; Leskes, M. Paramagnetic Metal-Ion Dopants as Polarization Agents for Dynamic Nuclear Polarization NMR Spectroscopy in Inorganic Solids. *ChemPhysChem* **2018**, *19* (17), 2139–2142.
- (36) Wolf, T.; Kumar, S.; Singh, H.; Chakrabarty, T.; Aussenac, F.; Frenkel, A. I.; Major, D. T.; Leskes, M. Endogenous Dynamic Nuclear Polarization for Natural Abundance ¹⁷O and Lithium NMR in the Bulk of Inorganic Solids. *J. Am. Chem. Soc.* **2019**, *141* (1), 451–462.
- (37) Carnahan, S. L.; Venkatesh, A.; Perras, F. A.; Wishart, J. F.; Rossini, A. J. High-Field Magic Angle Spinning Dynamic Nuclear Polarization Using Radicals Created by gamma-Irradiation. *J. Phys. Chem. Lett.* **2019**, *10* (17), 4770–4776.
- (38) Carnahan, S. L.; Chen, Y.; Wishart, J. F.; Lubach, J. W.; Rossini, A. J. Magic Angle Spinning Dynamic Nuclear Polarization Solid-State NMR Spectroscopy of gamma-Irradiated Molecular Organic Solids. *Solid State Nucl. Magn. Reson.* **2022**, *119*, 101785.
- (39) Fordyce, P.; Devries, K. L.; Fanconi, B. M. Chain Scission and Mechanical Degradation of Polystyrene. *Polym. Eng. Sci.* **1984**, *24* (6), 421–427.
- (40) Baytekin, H. T.; Baytekin, B.; Grzybowski, B. A. Mechanoradicals Created in “Polymeric Sponges” Drive Reactions in Aqueous Media. *Angew. Chem., Int. Ed. Engl.* **2012**, *51* (15), 3596–600.
- (41) Fitch, K. R.; Goodwin, A. P. Mechanochemical Reaction Cascade for Sensitive Detection of Covalent Bond Breakage in Hydrogels. *Chem. Mater.* **2014**, *26* (23), 6771–6776.
- (42) Zapp, C.; Obarska-Kosinska, A.; Rennekamp, B.; Kurth, M.; Hudson, D. M.; Mercadante, D.; Barayeu, U.; Dick, T. P.; Denysenkov, V.; Prisner, T.; et al. Mechanoradicals in Tensed Tendon Collagen as a Source of Oxidative Stress. *Nat. Commun.* **2020**, *11* (1), 2315.
- (43) Balema, V. P.; Wiench, J. W.; Pruski, M.; Pecharsky, P. K. Mechanically Induced Solid-State Generation of Phosphorus Ylides and the Solvent-Free Wittig Reaction. *J. Am. Chem. Soc.* **2002**, *124* (22), 6244–45.
- (44) Balema, V. P. Mechanical Processing-Experimental Tool or New Chemistry? *Ceram. Trans.* **2010**, *224*, 25–35.
- (45) Stolle, A.; Szuppa, T.; Leonhardt, S. E.; Ondruschka, B. Ball Milling in Organic Synthesis: Solutions and Challenges. *Chem. Soc. Rev.* **2011**, *40* (5), 2317–29.
- (46) Baig, R. B.; Varma, R. S. Alternative Energy Input: Mechanochemical, Microwave and Ultrasound-Assisted Organic Synthesis. *Chem. Soc. Rev.* **2012**, *41* (4), 1559–84.
- (47) Singh, N. K.; Hardi, N.; Balema, V. P. Mechanochemical Synthesis of an Yttrium Based Metal-Organic Framework. *Chem. Commun.* **2013**, *49* (10), 972–74.
- (48) Wang, G. W. Mechanochemical Organic Synthesis. *Chem. Soc. Rev.* **2013**, *42* (18), 7668–700.
- (49) Rightmire, N. R.; Hanusa, T. P. Advances in Organometallic Synthesis with Mechanochemical Methods. *Dalton Trans* **2016**, *45* (6), 2352–62.
- (50) Achar, T. K.; Bose, A.; Mal, P. Mechanochemical Synthesis of Small Organic Molecules. *Beilstein J. Org. Chem.* **2017**, *13*, 1907–1931.
- (51) Kubota, K.; Jiang, J.; Kamakura, Y.; Hisazumi, R.; Endo, T.; Miura, D.; Kubo, S.; Maeda, S.; Ito, H. Using Mechanochemistry to Activate Commodity Plastics as Initiators for Radical Chain Reactions of Small Organic Molecules. *J. Am. Chem. Soc.* **2024**, *146*, 1062–1070.
- (52) Lou, X.; Shen, M.; Li, C.; Chen, Q.; Hu, B. Reduction of the ¹³C Cross-Polarization Experimental Time for Pharmaceutical Samples with Long T1 by Ball Milling in Solid-State NMR. *Solid State Nucl. Magn. Reson.* **2018**, *94*, 20–25.
- (53) Metro, T. X.; Gervais, C.; Martinez, A.; Bonhomme, C.; Laurencin, D. Unleashing the Potential of ¹⁷O NMR Spectroscopy Using Mechanochemistry. *Angew. Chem., Int. Ed.* **2017**, *56* (24), 6803–6807.
- (54) Chen, C. H.; Gaillard, E.; Mentink-Vigier, F.; Chen, K.; Gan, Z.; Gaveau, P.; Rebiere, B.; Berthelot, R.; Florian, P.; Bonhomme, C.; Smith, M. E.; Metro, T. X.; Alonso, B.; Laurencin, D. Direct ¹⁷O Isotopic Labeling of Oxides Using Mechanochemistry. *Inorg. Chem.* **2020**, *59* (18), 13050–13066.
- (55) Lukin, S.; Tireli, M.; Stolar, T.; Barisic, D.; Blanco, M. V.; Di Michiel, M.; Uzarevic, K.; Halasz, I. Isotope Labeling Reveals Fast Atomic and Molecular Exchange in Mechanochemical Milling Reactions. *J. Am. Chem. Soc.* **2019**, *141* (3), 1212–1216.
- (56) Friscic, T.; Jones, W. Recent Advances in Understanding the Mechanism of Cocrystal Formation via Grinding. *Cryst. Growth Des.* **2020**, *9* (3), 1621–1637.
- (57) Kaupp, G. Mechanochemistry: the Varied Applications of Mechanical Bond-Breaking. *CrystEngComm* **2009**, *11* (3), 388–403.
- (58) Delori, A.; Friščić, T.; Jones, W. The Role of Mechanochemistry and Supramolecular Design in the Development of Pharmaceutical Materials. *CrystEngComm* **2012**, *14* (7), 2350.
- (59) Braga, D.; Maini, L.; Grepioni, F. Mechanochemical Preparation of Co-Crystals. *Chem. Soc. Rev.* **2013**, *42* (18), 7638–48.
- (60) Solares-Briones, M.; Coyote-Dotor, G.; Páez-Franco, J. C.; Zermeno-Ortega, M. R.; de la O Contreras, C. M.; Canseco-Gonzalez, D.; Avila-Sorros, A.; Morales-Morales, D.; German-Acacio, J. M. Mechanochemistry: A Green Approach in the Preparation of Pharmaceutical Cocrystals. *Pharmaceutics* **2021**, *13* (6), 790.
- (61) Weyna, D. R.; Shattock, T.; Vishweshwar, P.; Zaworotko, M. J. Synthesis and Structural Characterization of Cocrystals and Pharmaceutical Cocrystals: Mechanochemistry vs Slow Evaporation from Solution. *Cryst. Growth Des.* **2009**, *9* (2), 1106–1123.
- (62) Qiao, N.; Li, M.; Schlindwein, W.; Malek, N.; Davies, A.; Trappitt, G. Pharmaceutical Cocrystals: An Overview. *Int. J. Pharm.* **2011**, *419* (1–2), 1–11.
- (63) Li, J.; Nagamani, C.; Moore, J. S. Polymer Mechanochemistry: From Destructive to Productive. *Acc. Chem. Res.* **2015**, *48* (8), 2181–90.
- (64) Solala, I.; Henniges, U.; Pirker, K. F.; Rosenau, T.; Potthast, A.; Vuorinen, T. Mechanochemical Reactions of Cellulose and Styrene. *Cellulose* **2015**, *22* (5), 3217–3224.
- (65) Chen, Y.; Mellot, G.; van Luijk, D.; Creton, C.; Sijbesma, R. P. Mechanochemical Tools for Polymer Materials. *Chem. Soc. Rev.* **2021**, *50* (6), 4100–4140.
- (66) Balema, V. P.; Hlova, I. Z.; Carnahan, S. L.; Seyedi, M.; Dolotko, O.; Rossini, A. J.; Luzinov, I. Depolymerization of Polystyrene Under Ambient Conditions. *New J. Chem.* **2021**, *45* (6), 2935–2938.
- (67) Balema, V. P. Mechanical Processing in Hydrogen Storage Research and Development. *MRS Proc.* **2009**, *1209*, 1209–P0105.
- (68) Dolotko, O.; Hlova, I. Z.; Mudryk, Y.; Gupta, S.; Balema, V. P. Mechanochemical Recovery of Co and Li from LCO Cathode of Lithium-Ion Battery. *J. Alloys Compd.* **2020**, *824*, 153876.
- (69) Hlova, I. Z.; Singh, P.; Malynych, S. Z.; Gamernyk, R. V.; Dolotko, O.; Pecharsky, V. K.; Johnson, D. D.; Arroyave, R.; Pathak, A. K.; Balema, V. P. Incommensurate Transition-Metal Dichalcogenides via Mechanochemical Reshuffling of Binary Precursors. *Nanoscale Adv.* **2021**, *3* (14), 4065–71.
- (70) Rosay, M.; Tometich, L.; Pawsey, S.; Bader, R.; Schauwecker, R.; Blank, M.; Borchard, P. M.; Cauffman, S. R.; Felch, K. L.; Weber, R. T.; et al. Solid-State Dynamic Nuclear Polarization at 263 GHz: Spectrometer Design and Experimental Results. *Phys. Chem. Chem. Phys.* **2010**, *12* (22), 5850–60.
- (71) Cruickshank, P. A. S.; Bolton, D. R.; Robertson, D. A.; Hunter, R. I.; Wylde, R. J.; Smith, G. M. A Kilowatt Pulsed 94 GHz Electron Paramagnetic Resonance Spectrometer with High Concentration Sensitivity, High Instantaneous Bandwidth, and Low Dead Time. *Rev. Sci. Instrum.* **2009**, *80* (10), 103102.

- (72) Subramanya, M. V. H.; Marbey, J.; Kundu, K.; McKay, J. E.; Hill, S. Broadband Fourier-Transform-Detected EPR at W-Band. *Appl. Magn. Reson.* **2023**, *54*, 165–181.
- (73) Hassan, A. K.; Pardi, L. A.; Krzystek, J.; Sienkiewicz, A.; Goy, P.; Rohrer, M.; Brunel, L.-C. Ultrawide Band Multifrequency High-Field EMR Technique: A Methodology for Increasing Spectroscopic Information. *J. Magn. Reson.* **2000**, *142* (2), 300–312.
- (74) Stoll, S.; Ozarowski, A.; Britt, R. D.; Angerhofer, A. Atomic Hydrogen as High-Precision Field Standard for High-Field EPR. *J. Magn. Reson.* **2010**, *207* (1), 158–163.
- (75) Hlova, I. Z.; Dolotko, O.; Boote, B. W.; Pathak, A. K.; Smith, E. A.; Pecharsky, V. K.; Balema, V. P. Multi-Principal Element Transition Metal Dichalcogenides via Reactive Fusion of 3D-Heterostructures. *Chem. Commun. (Camb)* **2018**, *54* (89), 12574–12577.
- (76) Dolotko, O.; Hlova, I. Z.; Pathak, A. K.; Mudryk, Y.; Pecharsky, V. K.; Singh, P.; Johnson, D. D.; Boote, B. W.; Li, J.; Smith, E. A.; et al. Unprecedented Generation of 3D Heterostructures by Mechanochemical Disassembly and Re-ordering of Incommensurate Metal Chalcogenides. *Nat. Commun.* **2020**, *11* (1), 3005.
- (77) Olson, M.; Wheaton, J.; Okkema, M.; Oldham, N.; Martin, S. W. Optimized Thin Film Processing of Sodium Mixed Oxy-Sulfide-Nitride Glassy Solid Electrolytes for All-Solid-State Batteries. *ACS Appl. Energy Mater.* **2023**, *6* (11), 5842–5855.
- (78) Castle, J. G.; Feldman, D. W.; Klemens, P. G.; Weeks, R. A. Electron Spin-Lattice Relaxation at Defect Sites; E' Centers in Synthetic Quartz at 3 Kilo-Oersteds. *Phys. Rev.* **1963**, *130* (2), 577–588.
- (79) Cacaina, D.; Ylanen, H.; Uduar, D. A.; Simon, S. EPR Study of gamma Irradiated Yttrium Bioactive Glasses and Yttrium Silica Sol-Gel Microspheres. *J. Optoelectron. Adv. Mater.* **2007**, *9* (3), 675–679.
- (80) Tiño, J.; Čapla, M.; Szöcs, F. ESR Study of Radicals Trapped in Mechanically Degraded Polystyrene. *Eur. Polym. J.* **1970**, *6*, 397–401.
- (81) Stefanovic, B.; Pirker, K. F.; Rosenau, T.; Potthast, A. Effects of tribochemical treatments on the integrity of cellulose. *Carbohydr. Polym.* **2014**, *111*, 688–699.
- (82) Kmiec, S.; Joyce, A.; Bayko, D.; Martin, S. W. Glass Formation and Structure of Melt Quenched Mixed Oxy-Sulfide Na₄P₂S₇-xOx Glasses for 0 ≤ x ≤ 5. *J. Non-Cryst. Solids* **2020**, *534*, 119776.
- (83) Joyce, A.; Kmiec, S.; Martin, S. W. Glass Transition Temperature Studies of Planetary Ball Milled Glasses: Accessing the Rapidly Cooled Glassy State in Na₄P₂S₇-xOx, 0 ≤ x ≤ 7, Oxy-thio Phosphate Glasses. *J. Non-Cryst. Solids* **2021**, *551*, 120462.
- (84) Gogoi, P. K.; Hu, Z.; Wang, Q.; Carvalho, A.; Schmidt, D.; Yin, X.; Chang, Y. H.; Li, L. J.; Sow, C. H.; Neto, A. H. C.; et al. Oxygen Passivation Mediated Tunability of Trion and Excitons in MoS₂. *Phys. Rev. Lett.* **2017**, *119* (7), 077402.
- (85) Bretscher, H.; Li, Z.; Xiao, J.; Qiu, D. Y.; Refaely-Abramson, S.; Alexander-Webber, J. A.; Tanoh, A.; Fan, Y.; Delpont, G.; Williams, C. A.; et al. Rational Passivation of Sulfur Vacancy Defects in Two-Dimensional Transition Metal Dichalcogenides. *ACS Nano* **2021**, *15* (5), 8780–8789.
- (86) Liang, Q.; Zhang, Q.; Zhao, X.; Liu, M.; Wee, A. T. S. Defect Engineering of Two-Dimensional Transition-Metal Dichalcogenides: Applications, Challenges, and Opportunities. *ACS Nano* **2021**, *15* (2), 2165–2181.
- (87) Lubach, J. W.; Xu, D.; Segmuller, B. E.; Munson, E. J. Investigation of the Effects of Pharmaceutical Processing Upon Solid-State NMR Relaxation Times and Implications to Solid-State Formulation Stability. *J. Pharm. Sci.* **2007**, *96*, 777–787.
- (88) Dempah, K. E.; Barich, D. H.; Kaushal, A. M.; Zong, Z.; Desai, S. D.; Suryanarayanan, R.; Kirsch, L.; Munson, E. J. Investigating Gabapentin Polymorphism Using Solid-State NMR Spectroscopy. *AAPS PharmSciTech* **2013**, *14*, 19–28.
- (89) Dempah, K. E.; Lubach, J. W.; Munson, E. J. Characterization of the Particle Size and Polydispersity of Dicumarol Using Solid-State NMR Spectroscopy. *Mol. Pharmaceutics* **2017**, *14*, 856–865.
- (90) Lou, X.; Shen, M.; Li, C.; Chen, Q.; Hu, B. Reduction of the ¹³C Cross-Polarization Experimental Time for Pharmaceutical Samples with Long T1 by Ball Milling in Solid-State NMR. *Solid State Nucl. Magn. Reson.* **2018**, *94*, 20–25.
- (91) Hennart, S. L. A.; van Hee, P.; Drouet, V.; Domingues, M. C.; Wildeboer, W. J.; Meesters, G. M. H. Characterization and Modeling of a Sub-Micron Milling Process Limited by Agglomeration Phenomena. *Chem. Eng. Sci.* **2012**, *71*, 484–495.
- (92) Harbridge, J. R.; Rinard, G. A.; Quine, R. W.; Eaton, S. S.; Eaton, G. R. Enhanced Signal Intensities Obtained by Out-of-Phase Rapid-Passage EPR for Samples with Long Electron Spin Relaxation Times. *J. Magn. Reson.* **2002**, *156* (1), 41–51.
- (93) Perras, F. A.; Raju, M.; Carnahan, S. L.; Akbarian, D.; van Duin, A. C. T.; Rossini, A. J.; Pruski, M. Full-Scale Ab Initio Simulation of Magic-Angle-Spinning Dynamic Nuclear Polarization. *J. Phys. Chem. Lett.* **2020**, *11* (14), 5655–5660.